


Article

# Anion-Dominated Copper Salicyaldimine Complexes—Structures, Coordination Mode of Nitrate and Decolorization Properties toward Acid Orange 7 Dye

Meng-Jung Tsai, Chi-Jou Tsai, Ken Lin and Jing-Yun Wu \* 

Department of Applied Chemistry, National Chi Nan University, Nantou 545, Taiwan;  
s97324905@mail1.ncnu.edu.tw (M.-J.T.); tgb751@hotmail.com (C.-J.T.); rivenate1009@gmail.com (K.L.)

\* Correspondence: jyunwu@ncnu.edu.tw

Received: 24 July 2020; Accepted: 22 August 2020; Published: 24 August 2020



**Abstract:** A salicyaldimine ligand, 3-tert-butyl-4-hydroxy-5-(((pyridin-2-ylmethyl)imino)methyl)benzoic acid ( $H_2L_{\text{salpyca}}$ ) and two Cu(II)–salicyaldimine complexes,  $[Cu(HL_{\text{salpyca}})Cl]$  (**1**) and  $[Cu(HL_{\text{salpyca}})(NO_3)]_n$  (**2**), have been synthesized. Complex **1** has a discrete mononuclear structure, in which the Cu(II) center is in a distorted square-planar geometry made up of one  $HL_{\text{salpyca}}^-$  monoanion in an NNO tris-chelating mode and one  $Cl^-$  anion. Complex **2** adopts a neutral one-dimensional zigzag chain structure propagating along the crystallographic [010] direction, where the Cu(II) center suits a distorted square pyramidal geometry with a  $\tau$  value of 0.134, consisted of one  $HL_{\text{salpyca}}^-$  monoanion as an NNO tris-chelator and two  $NO_3^-$  anions. When the Cu...O semi coordination is taken into consideration, the nitrate ligand bridges two Cu(II) centers in an unsymmetrical bridging-tridentate with a  $\mu, \kappa^4 O, O': O', O''$  coordination. Clearly, anion herein plays a critical role in dominating the formation of discrete and polymeric structures of copper salicyaldimine complexes. Noteworthy, complex **2** is insoluble but highly stable in  $H_2O$  and various organic solvents ( $CH_3OH$ ,  $CH_3CN$ , acetone,  $CH_2Cl_2$  and THF). Moreover, complex **2** shows good photocatalytic degradation activity and recyclability to accelerate the decolorization rate and enhance the decolorization performance of acid orange 7 (AO7) dye by hydrogen peroxide ( $H_2O_2$ ) under daylight.

**Keywords:** acid orange 7; anion effect; copper; nitrate; degradation

## 1. Introduction

Salicyaldimine derivatives with the NO donor set of azomethine nitrogen and phenolato oxygen have been extensively studied in coordination chemistry due to their preparational accessibilities and their versatility in terms of steric and electronic modifications [1–5]. Metal–salicyaldimine complexes so far have achieved a remarkable success in structure variation including traditional coordination complexes [2–4,6,7] and metallosupramolecular architectures such as discrete macrocycles [8,9], helicates [10,11] and coordination polymers [12–15]. Moreover, metal–salicyaldimine complexes have wide applications in fields such as catalysis [5,15,16], molecular magnetism [7,17] and fluorescent chemosensors [18,19].

On the other hand, the presence of organic pollutants, such as azo dyes, the most diverse group of synthetic dyes used in food, textile and printing industries, in water streams is becoming a seriously environmental problem due to the fact of their color, toxicity, potential carcinogenicity and non-biodegradable nature [20–24]. Therefore, the treatment of dye-containing wastewater is a matter of great important issue for environmental protection and has attracted worldwide attention. Nowadays,

adsorptive removal (non-destructive process) [25,26] and degradation (destructive process) [27,28] are the two most promising techniques widely utilized in the decolorization of dye-contaminated water owing to their advantages of mild operation conditions, convenience, high efficiency and relative low costs [20,22–24,29–31].

In recent years, our group has reported several transition metal complexes of salicyaldimine Schiff base ligands with NO and N<sub>2</sub>O donor sets, which have represented mononuclear molecular structures and one- and two-dimensional periodical structures (1D chain and 2D layer) with interesting structural and photophysical properties [14,32,33]. Further, our group has also contributed efforts in the decolorization of aqueous solutions of organic dyes through the adsorptive removal process [34–37]. As a continuation, we report herein the synthesis and structures of two new Cu(II)–salicyaldimine complexes, [Cu(HL<sub>salpyca</sub>)Cl] (**1**, H<sub>2</sub>L<sub>salpyca</sub> = 3-*tert*-butyl-4-hydroxy-5-(((pyridin-2-ylmethyl)imino)methyl)benzoic acid) and [Cu(HL<sub>salpyca</sub>)(NO<sub>3</sub>)<sub>n</sub>] (**2**). Complex **1** shows a mononuclear structure while complex **2** has a 1D zigzag chain structure. Such structural diversities are tentatively ascribed to the influence of anion. It is also noted that the nitrate in **2** suits a bridging–tridentate ligand with a coordination mode of  $\mu, \kappa^4 O, O':O'', O''$  to bridge two Cu(II) ions to form the extended structure. Moreover, complex **2** is very stable in H<sub>2</sub>O and would cooperate with H<sub>2</sub>O<sub>2</sub> to show remarkable photocatalytic activity toward degradation of acid orange 7 (AO7) under daylight.

## 2. Experimental Section

### 2.1. Materials and Methods

Chemical reagents were of reagent grade quality obtained from commercial sources (Alfa Aesar, Heysham, UK; ACROS, Pittsburgh, PA, USA; SHOWA, Saitama, Japan) and used as received without further purification. 5-*tert*-Butyl-3-formyl-4-hydroxybenzoic acid [38,39] were synthesized according to the reported literature. Proton nuclear magnetic resonance (<sup>1</sup>H NMR) spectra were collected at room temperature by using a Bruker AMX-300 Solution-NMR spectrometer (Bruker, New Taipei, Taiwan) operating at 300 MHz. Chemical shifts are reported in parts per million (ppm) with reference to the residual protons of the deuterated solvent and coupling constants are given in hertz (Hz). Mass spectra were recorded by using a Bruker Daltonics flexAnalysis matrix-assisted laser desorption/ionization time of flight (MALDI-TOF) mass spectrometer (Bruker, New Taipei, Taiwan). Thermogravimetric (TG) analyses were carried out under a flux of nitrogen by using a Thermo Cahn VersaTherm HS TG analyzer (Thermo, Newington, NH, USA) at a heating rate of 5 °C per minute from 25 to 900 °C. X-ray powder diffraction (XRPD) patterns were acquired on a Shimadzu XRD-7000 diffractometer (Shimadzu, Kyoto, Japan) with a graphite monochromatized Cu K $\alpha$  radiation ( $\lambda = 1.5406 \text{ \AA}$ ; 40 kV, 30 mA) at a scan speed of 1.2° per minute. Infrared (IR) spectra were collected on a Perkin-Elmer Frontier Fourier transform infrared spectrometer (Perkin-Elmer, Taipei, Taiwan) in the 4000–500 cm<sup>−1</sup> region using attenuated total reflection (ATR) technique. Microanalyses were carried out by using an Elementar Vario EL III analytical instrument (Elementar, Langenselbold, Germany). UV-vis absorption spectra were recorded on a JASCO V-750 UV/VIS spectrophotometer (JASCO, Tokyo, Japan). Fluorescence spectra were recorded at room temperature on a Hitachi F7000 fluorescence spectrophotometer (Hitachi, Tokyo, Japan). Inductively coupled plasma optical emission spectrometry (ICP-OES) analyses were conducted on an Agilent 5100 ICP-OES instrument (Agilent, Santa Clara, CA, US).

### 2.2. Synthesis of 3-*Tert*-butyl-4-hydroxy-5-(((pyridin-2-ylmethyl)imino)methyl)benzoic Acid (H<sub>2</sub>L<sub>salpyca</sub>)

To a methanolic solution (2 mL) of 2-(aminomethyl)pyridine (0.10 g, 1.0 mmol), a methanolic solution (6 mL) of 5-*tert*-butyl-3-formyl-4-hydroxybenzoic acid (0.22 g, 1.0 mmol) was added under nitrogen atmosphere. The solution was stirred for 2 h at room temperature. After the solvent was removed under reduced pressure, yellow powdered product of H<sub>2</sub>L<sub>salpyca</sub> was obtained in a yield

of 54% (0.17 g, 0.54 mmol).  $^1\text{H}$  NMR (300 MHz,  $\text{DMSO-}d_6$ , ppm):  $\delta$  8.81 (s, 1H), 8.56 (d,  $J = 4.8$  Hz, 1H), 7.96 (s, 1H), 7.86–7.80 (m, 2H), 7.44 (d,  $J = 7.8$  Hz, 1H), 7.36–7.31 (m, 1H), 4.92 (s, 2H), 1.34 (s, 9H) (Figure S1). MS (MALDI-TOF):  $m/z$  312.878  $[\text{M} + \text{H}]^+$  (calcd for  $\text{C}_{18}\text{H}_{20}\text{N}_2\text{O}_3$ :  $m/z$  312.18) (Figure S2). IR (ATR,  $\text{cm}^{-1}$ ): 3425, 1961, 2924, 2862, 1956, 1677, 1632, 1602, 1477, 1392, 1364, 4334, 1307, 1279, 1239, 1202, 1179, 1120, 1014, 946, 879, 839, 804, 767, 705, 674, 602. Anal. Calcd for  $\text{C}_{18}\text{H}_{20}\text{N}_2\text{O}_3$ : C, 69.21; H, 6.45; N, 8.97%. Found: C, 69.14; H, 6.29; N, 8.68%.

### 2.3. Synthesis of $[\text{Cu}(\text{HL}_{\text{salpyca}})\text{Cl}]$ (**1**)

A methanolic solution (1 mL) of  $\text{H}_2\text{L}_{\text{salpyca}}$  (31.2 mg, 0.10 mmol) and an aqueous solution (1 mL) of  $\text{CuCl}_2$  (13.4 mg, 0.10 mmol) were sealed in a Teflon-lined stainless steel container. The container was heated at 80 °C for 12 h and then cooled to 30 °C. Green needle-shaped crystals of **1** were obtained in a yield of 39% (16.3 mg,  $3.9 \times 10^{-2}$  mmol). MS (MALDI-TOF):  $m/z$  410.806  $[\text{M}]^+$  (calcd for  $\text{C}_{18}\text{H}_{19}\text{N}_2\text{O}_3\text{ClCu}$ :  $m/z$  410.34) (Figure S3). IR (ATR,  $\text{cm}^{-1}$ ): 3065, 2961, 2908, 2869, 2568, 1672, 1596, 1536, 1484, 1407, 1355, 1263, 1258, 1230, 1173, 1052, 996, 921, 824, 795, 761, 697, 658. TGA: 200 °C (decomp.). Anal. Calcd for  $\text{C}_{18}\text{H}_{19}\text{N}_2\text{O}_3\text{ClCu}$ : C, 52.68; H, 4.67; N, 6.83%. Found: C, 52.88; H, 4.39; N, 6.89%.

### 2.4. Synthesis of $[\text{Cu}(\text{HL}_{\text{salpyca}})(\text{NO}_3)]_n$ (**2**)

A methanolic solution (0.5 mL) of  $\text{H}_2\text{L}_{\text{salpyca}}$  (31.2 mg, 0.10 mmol) and an aqueous solution (1.5 mL) of  $\text{Cu}(\text{NO}_3)_2 \cdot 2.5\text{H}_2\text{O}$  (23.2 mg, 0.10 mmol) were sealed in a Teflon-lined stainless steel container. The container was heated at 80 °C for 12 h and then cooled to 30 °C. Green needle-shaped crystals of **2** were obtained in a yield of 28% (12.2 mg,  $2.8 \times 10^{-2}$  mmol). IR (ATR,  $\text{cm}^{-1}$ ): 3431, 2928, 2590, 2003, 1682, 1629, 1600, 1573, 1532, 1488, 1475, 1440, 1413, 1394, 1354, 1331, 1274, 1244, 1216, 1191, 1065, 1054, 1029, 1004, 948. TGA: 215 °C (decomp.). Anal. Calcd for  $\text{C}_{18}\text{H}_{19}\text{N}_3\text{O}_6\text{Cu}$ : C, 49.48; H, 4.38; N, 9.62%. Found: C, 49.45; H, 4.66; N, 9.47%.

### 2.5. X-Ray Data Collection and Structure Refinement

Quality crystals of **1** and **2** were obtained for single-crystal structure determination. Data collections were performed on an Oxford Diffraction Gemini S diffractometer for **1** and on a Bruker D8 Venture diffractometer for **2**. Both diffractometers are equipped with a graphite monochromated  $\text{Mo K}\alpha$  radiation ( $\lambda = 0.71073$  Å). Starting models for structure refinement were found using direct methods with SHELXS-97 program [40] and the structural data were refined by full-matrix least-squares methods against  $F^2$  using the SHELXL-2014/7 [41], incorporated in WINGX-v2014.1 [42] crystallographic collective package. All non-hydrogen atoms were found from the different Fourier maps and refined anisotropically. Carbon-bound hydrogen atoms were placed by geometrical calculation and refined as riding mode. Oxygen-bound hydrogen atoms were located in a difference Fourier map and the positional parameters were refined, with the restraint  $\text{O-H} = 0.82(1)$  Å. Isotropic displacement parameters of all hydrogen atoms were derived from the parent atoms. ORTEP plots and crystal structure drawings for **1** and **2** were drawn using the Diamond software [43]. CCDC 1955728–1955729 contain the supplementary crystallographic data for this paper. These data can be obtained free of charge via <http://www.ccdc.cam.ac.uk/conts/retrieving.html> or from the Cambridge Crystallographic Data Centre, 12 Union Road, Cambridge CB2 1EZ, UK; fax: (+44) 1223-336-033; or e-mail: deposit@ccdc.cam.ac.uk. Detailed crystallographic data are summarized in Table 1. Selected bond lengths and angles are listed in Table 2 and important hydrogen-bonding parameters are shown in Table 3.

**Table 1.** Crystallographic data for **1** and **2**.

Complex	1	2
Empirical formula	C <sub>18</sub> H <sub>19</sub> ClCuN <sub>2</sub> O <sub>3</sub>	C <sub>18</sub> H <sub>19</sub> CuN <sub>3</sub> O <sub>6</sub>
<i>M<sub>w</sub></i>	410.34	436.90
Crystal system	Triclinic	Monoclinic
Space group	<i>P</i> $\bar{1}$	<i>P</i> 2 <sub>1</sub> / <i>c</i>
<i>a</i> (Å)	8.2742 (7)	13.8487 (7)
<i>b</i> (Å)	8.5837 (7)	8.2653 (4)
<i>c</i> (Å)	12.6658 (9)	16.2531 (8)
$\alpha$ (°)	99.124 (6)	90
$\beta$ (°)	90.116 (6)	97.386 (2)
$\gamma$ (°)	102.508 (7)	90
<i>V</i> (Å <sup>3</sup> )	866.49 (12)	1844.95 (16)
<i>Z</i>	2	4
<i>T</i> (K)	150(2)	150 (2)
$\lambda$ (Å)	0.71073	0.71073
<i>D<sub>calc</sub></i> (g cm <sup>-3</sup> )	1.573	1.573
<i>F</i> <sub>000</sub>	422	900
$\mu$ (mm <sup>-1</sup> )	1.434	1.226
$\theta_{min}, \theta_{max}$ (deg)	2.952, 29.356	2.966, 26.431
<i>R</i> <sub>1</sub> <sup>a</sup> ( <i>I</i> > 2 $\sigma$ ( <i>I</i> ))	0.0327	0.0411
<i>wR</i> <sub>2</sub> <sup>b</sup> ( <i>I</i> > 2 $\sigma$ ( <i>I</i> ))	0.0738	0.1061
<i>R</i> <sub>1</sub> <sup>a</sup> (all data)	0.0398	0.0563
<i>wR</i> <sub>2</sub> <sup>b</sup> (all data)	0.0780	0.1250
GOF on <i>F</i> <sup>2</sup>	1.046	1.169

<sup>a</sup>  $R_1 = \sum ||F_o| - |F_c|| / \sum |F_o|$ . <sup>b</sup>  $wR_2 = [\sum w(F_o^2 - F_c^2)^2 / \sum w(F_o^2)^2]^{1/2}$ .  $w = 1/[\sigma^2(F_o^2) + (ap)^2 + (bp)]$ ,  $p = (F_o^2 + 2F_c^2)/3$ . For **1**,  $a = 0.0270$ ,  $b = 0.4203$ ; For **2**,  $a = 0.0581$ ,  $b = 2.4290$ .

**Table 2.** Selected bond lengths (Å) and angles (°) in **1** and **2**<sup>a</sup>.

1			
Cu1–Cl2	2.2299 (6)	Cu1–O1	1.8857 (14)
Cu1–N1	1.9376 (17)	Cu1–N2	1.9971 (17)
O1–Cu1–N1	92.00 (6)	O1–Cu1–N2	165.35 (7)
N1–Cu1–N2	82.99 (7)	O1–Cu1–Cl2	90.81 (5)
N1–Cu1–Cl2	164.08 (6)	N2–Cu1–Cl2	97.79 (5)
2			
Cu1–O1	1.892 (2)	Cu1–N1	1.931 (2)
Cu1–N2	1.994 (3)	Cu1–O4	2.019 (2)
Cu1–O5#1	2.437 (3)		
O1–Cu1–N1	93.00 (9)	O1–Cu1–N2	176.25 (9)
N1–Cu1–N2	83.45 (10)	O1–Cu1–O4	89.81 (9)
N1–Cu1–O4	168.19 (10)	N2–Cu1–O4	93.43 (10)
O1–Cu1–O5#1	95.63 (9)	N1–Cu1–O5#1	120.20 (9)
N2–Cu1–O5#1	87.21 (10)	O4–Cu1–O5#1	70.84 (8)

<sup>a</sup> Symmetry code: For **2**, #1,  $-x, y + 1/2, -z + 1/2$ .

**Table 3.** Hydrogen bonding parameters in **1** and **2** (D, Donor atom; A, Acceptor atom)<sup>a</sup>.

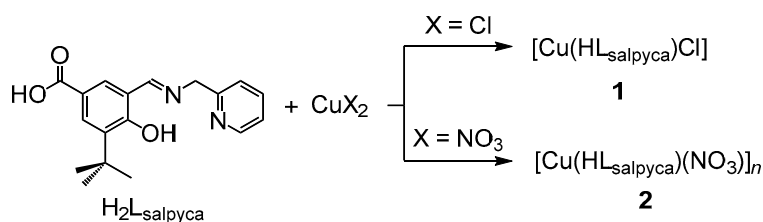
D–H...A	d(D–H) (Å)	d(H...A) (Å)	d(D...A) (Å)	$\angle$ (D–H...A) (°)
1				
O3–H3...O2#1	0.81 (2)	1.84 (2)	2.637 (2)	168 (3)
C9–H9B...Cl2#2	0.97	2.70	3.567 (3)	150
2				
O3–H3...O2#2	0.82 (3)	1.81 (3)	2.633 (3)	174 (4)

<sup>a</sup> Symmetry code: **1**, #1,  $-1 - x, -y, -z$ ; #2,  $-1 + x, y, z$ . **2**, #1,  $1 - x, 2 - y, -z$ .

### 3. Results and Discussion

#### 3.1. Syntheses and Characterization

Complexes **1** and **2** were synthesized from the reactions of copper(II) salts ( $\text{CuCl}_2$  and  $\text{Cu}(\text{NO}_3)_2 \cdot 2.5\text{H}_2\text{O}$ ) and  $\text{H}_2\text{L}_{\text{salpyca}}$  under hydro(solvo)thermal conditions at  $80^\circ\text{C}$  for 12 h (Scheme 1). Their molecular structures have been determined by the single-crystal X-ray structure analyses and their bulky samples have been characterized to be a single crystalline phase through X-ray powder diffraction (XRPD) measurements (Figure S4).



Scheme 1. Synthesis of complexes **1** and **2**.

#### 3.2. Crystal Structural Description of $[\text{Cu}(\text{HL}_{\text{salpyca}})\text{Cl}]$ (**1**)

Complex **1** crystallizes in the triclinic space group  $P\bar{1}$  and the asymmetric unit consists of one Cu(II) center, one  $\text{HL}_{\text{salpyca}}^-$  monoanion and one  $\text{Cl}^-$  anion. The Cu(II) center is tris-chelated by one  $\text{HL}_{\text{salpyca}}^-$  monoanion through its phenolato, imino and pyridine groups and further coordinated by one  $\text{Cl}^-$  anion, furnishing a distorted square-planar geometry (Figure 1a), with the Cu and the Cl away from the plane 0.24 and 1.11 Å, respectively. The carboxyl group of the  $\text{HL}_{\text{salpyca}}^-$  ligand is protonated and non-coordinated. The Cu– $\text{N}_{\text{pyridine}}$ , Cu– $\text{N}_{\text{imino}}$ , Cu– $\text{O}_{\text{phenolato}}$  and Cu–Cl bond lengths are 1.9971(17), 1.9376(17), 1.8857(14) and 2.2299(6) Å, respectively and the  $\text{N}_{\text{pyridine}}\text{–Cu–N}_{\text{imino}}$  and  $\text{N}_{\text{imino}}\text{–Cu–O}_{\text{phenolato}}$  bond angles are  $82.98(7)$  and  $92.00(6)^\circ$ , respectively. Two  $[\text{Cu}(\text{HL}_{\text{salpyca}})\text{Cl}]$  molecules form a hydrogen-bonded dimer through intermolecular hydrogen bonds ( $\text{O}3\text{–H}3\cdots\text{O}2\#1$ ,  $d(\text{D}\cdots\text{A}) = 2.637(2)$  Å,  $\angle(\text{D–H}\cdots\text{A}) = 168(3)^\circ$ ,  $\#1 = -1 - x, -y, -z$ ) between two carboxyl groups of two  $\text{HL}_{\text{salpyca}}^-$  ligands, with a graph set of  $\text{R}_2^2(8)$  (Figure 1b) [44]. In addition, there are also intermolecular  $\pi\cdots\pi$  interactions (plane $\cdots$ plane: 3.37 and 3.69 Å) between any two neighboring  $[\text{Cu}(\text{HL}_{\text{salpyca}})\text{Cl}]$  molecules that stack in a column manner along the crystallographic [010] direction, that is,  $b$  axis (Figure 1c). Moreover, there are also weak but significant intermolecular C–H $\cdots$ Cl interactions ( $\text{C}9\text{–H}9\text{B}\cdots\text{Cl}2\#2$ ,  $d(\text{D}\cdots\text{A}) = 3.567(3)$  Å,  $\angle(\text{D–H}\cdots\text{A}) = 150^\circ$ ,  $\#1 = -1 + x, y, z$ ) between the chloro ligands and the methylene moieties of the  $\text{HL}_{\text{salpyca}}^-$  ligands (Figure 1d).

#### 3.3. Crystal Structural Description of $[\text{Cu}(\text{HL}_{\text{salpyca}})(\text{NO}_3)]_n$ (**2**)

Complex **2** crystallizes in the monoclinic space group  $P2_1/c$  and has an infinite zigzag chain structure. The asymmetric unit consists of one Cu(II) center, one  $\text{HL}_{\text{salpyca}}^-$  monoanion and one  $\text{NO}_3^-$  anion. The Cu(II) center is coordinated by one  $\text{HL}_{\text{salpyca}}^-$  monoanion as a tris-chelator through its phenolato, imino and pyridine groups and further coordinated to two  $\text{NO}_3^-$  anion (Figure 2a), furnishing a distorted square pyramidal geometry, with a  $\tau$  value of 0.134 [45]. The carboxyl group of the  $\text{HL}_{\text{salpyca}}^-$  ligand is protonated and non-coordinated. The Cu– $\text{N}_{\text{pyridine}}$ , Cu– $\text{N}_{\text{imino}}$ , Cu– $\text{O}_{\text{phenolato}}$  and Cu– $\text{O}_{\text{nitrato}}$  bond lengths are 1.994(3), 1.931(2), 1.892(2) and 2.019(2)/2.437(3) Å, respectively and the  $\text{N}_{\text{pyridine}}\text{–Cu–N}_{\text{imino}}$  and  $\text{N}_{\text{imino}}\text{–Cu–O}_{\text{phenolato}}$  bond angles are  $83.45(10)$  and  $93.00(9)^\circ$ , respectively. Basically, the nitrato ligand adopts a bridging-bidentate with a semi-coordination ( $\mu, \kappa^2\text{O}, \text{O}'$ ). However, when the Cu $\cdots$ O semi-coordination ( $\text{Cu}1\cdots\text{O}6 = 2.73$  Å,  $\text{Cu}1\cdots\text{O}4\#1 = 3.01$ ,  $\#1 = -x, y + 1/2, -z + 1/2$ ) is taken into consideration, the nitrato ligand suits an unsymmetrical bridging-tridentate with a  $\mu, \kappa^4\text{O}, \text{O}'\text{:O}', \text{O}''$  coordination, with a Cu $\cdots$ Cu separation of 4.97 Å, among various possible coordination modes of nitrato ligand [46–51]. Morozov and coworkers have shown that nitrato ligand exhibits 28 coordination modes that are classified in terms of the number of oxygen atoms used by the nitrato

ligand for binding to complexing metal centers [52]. Based on the definition, M, B and T denote one, two and three nitrate O atoms used for binding, respectively and the superscripts mean the number of metal atoms connected to one nitrate O atom (the first superscript) or two nitrate O atoms (the second superscript). Accordingly, the coordination mode of nitrate ligand in complex **2** is classified to be T<sup>02</sup> (Scheme 2, mode V).

Each nitrate ligand bridges two [Cu(HL<sub>salpyca</sub>)]<sup>+</sup> cationic motifs to generate a neutral 1D zigzag chain structure that propagates along the crystallographic [010] direction, that is, the *b* axis (Figure 2b). There are chain-to-chain hydrogen bonds (O3–H3···O2#2,  $d(D\cdots A) = 2.633(3) \text{ \AA}$ ,  $\angle(D-H\cdots A) = 173^\circ$ , #2 = 1 – *x*, 2 – *y*, –*z*) between two carboxyl groups of two HL<sub>salpyca</sub><sup>–</sup> ligands, with a graph set of R<sub>2</sub><sup>2</sup>(8) [44], in adjacent chains (Figure 2c). As a result, a hydrogen-bonded 2D wavy sheet is formed (Figure 2d). This structure is compared to a zigzag chain structure of the Cu(II)–salicylaldimine complex {[Cu(salpyca)]·3H<sub>2</sub>O}<sub>*n*</sub> (where H<sub>2</sub>salpyca = 4-hydroxy-3-(((pyridin-2-yl)methylimino)methyl)benzoic acid) [33], prepared from a solvent-mediated cation-exchange of [Zn(salpyca)(H<sub>2</sub>O)]<sub>*n*</sub> and Cu(NO<sub>3</sub>)<sub>2</sub>·6H<sub>2</sub>O in aqueous solution, where the salpyca<sup>2–</sup> displays not only the NNO tris-chelating mode from its pyridine, imino and phenolato groups but also bridging behavior through its monodentately-carboxylato group.

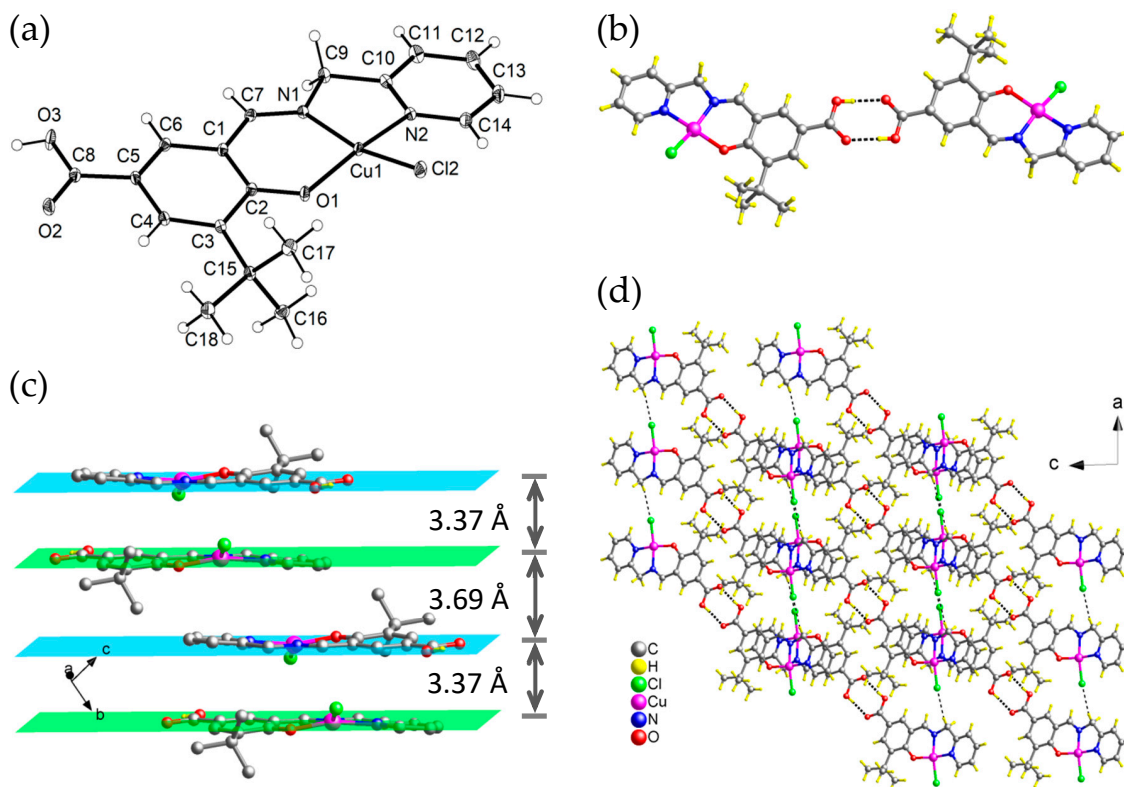


**Figure 1.** (a) ORTEP plot of **1** (30% probability ellipsoid) (b) A hydrogen-bonded dimer of [Cu(HL<sub>salpyca</sub>)Cl] generated from the R<sub>2</sub><sup>2</sup>(8) hydrogen-bonding pattern. (c) Representation of intermolecular  $\pi\cdots\pi$  interactions (plane $\cdots$ plane: 3.37 and 3.69 Å) between any two neighboring [Cu(HL<sub>salpyca</sub>)Cl] molecules in **1**. (d) Packing diagram of **1**, showing O<sub>carboxyl</sub>–H $\cdots$ O<sub>carboxyl</sub> and C–H $\cdots$ Cl hydrogen-bonding interactions (dashed lines).

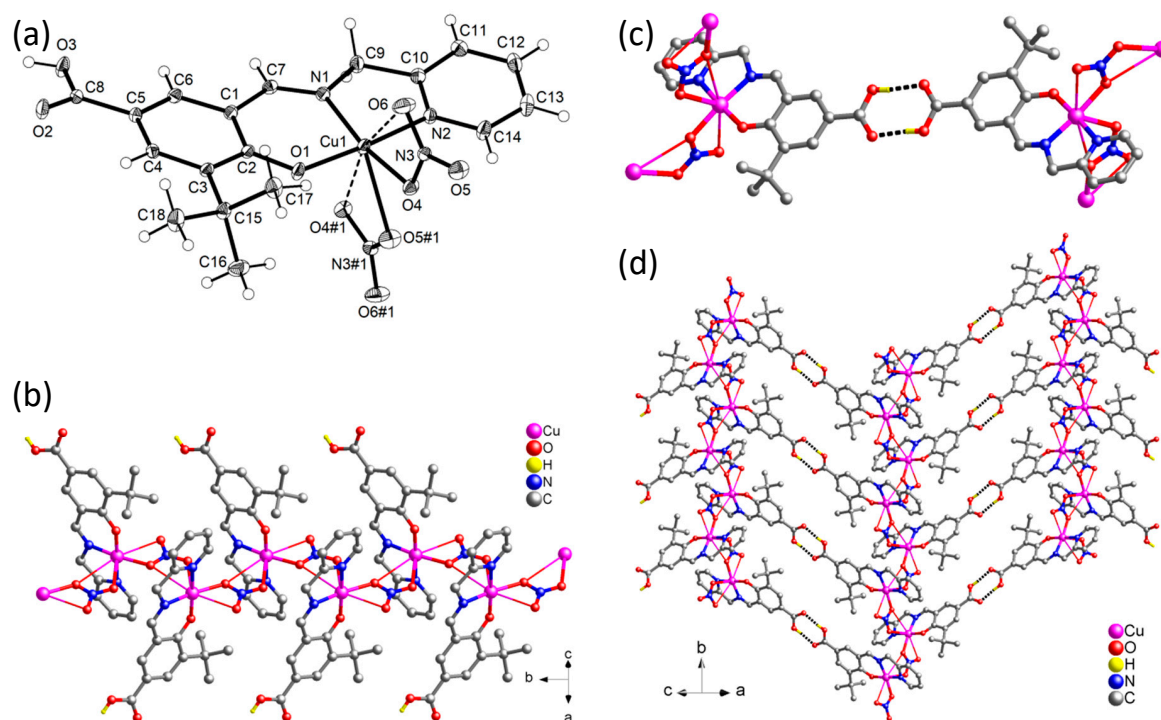
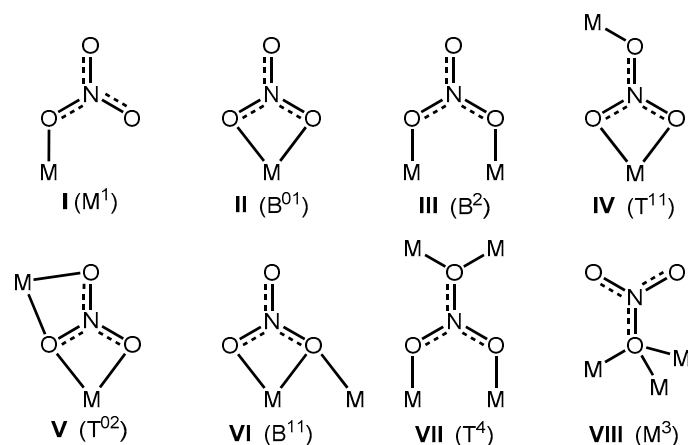


**Figure 2.** Crystal structure of **2**: (a) ORTEP plot of the coordination environment around the Cu(II) center (30% probability ellipsoid). Weak Cu...O semi-coordinations are shown as dashed lines. Symmetry code: #1,  $-x, y + 1/2, -z + 1/2$ . (b) View of the 1D zigzag chain structure. (c) Highlight the  $R_2^2(8)$  hydrogen-bonding pattern between two carboxyl groups of two  $HL_{salpyca}^-$  ligands in two neighboring chains. (d) A 2D supramolecular wavy sheet supported by  $O_{carboxyl}-H \cdots O_{carboxyl}$  hydrogen bonds (dashed lines).



**Scheme 2.** Some possible coordination modes of nitrate ligands. The terms shown in parentheses are the coordination modes described by Morozov notation. Adapted from [52], with permission from Springer Nature, 2009.

### 3.4. Thermogravimetric (TG) Analysis

The thermogravimetric (TG) traces of **1** and **2** both showed a long plateau before a decomposition process occurred at temperature approaching 200 and 215 °C, respectively (Figure 3). For **2**, after a two-step decomposition of the framework ended at a temperature approaching 509 °C, a weight of 17.8% of the total sample was left which is reasonably assigned to CuO (calcd. 18.2%).

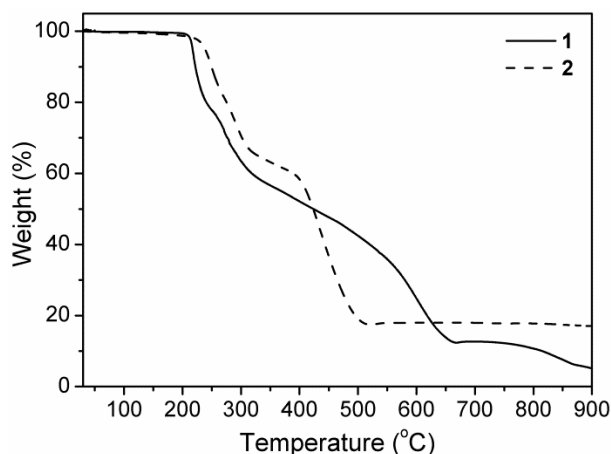


Figure 3. The thermogravimetric (TG) diagrams of 1 and 2.

### 3.5. Stability of 2

The chemical stability of zigzag chain 2 in crystalline phase has been examined. As observation, 2 displayed high chemical stability to maintain the framework integrity and crystallinity after immersing in H<sub>2</sub>O, methanol (CH<sub>3</sub>OH), acetonitrile (CH<sub>3</sub>CN), acetone, dichloromethane (CH<sub>2</sub>Cl<sub>2</sub>) and tetrahydrofuran (THF), respectively, for 1 day. This is supported by the checked XRPD profiles which are almost identical with that of as-synthesized crystalline samples (Figure 4).

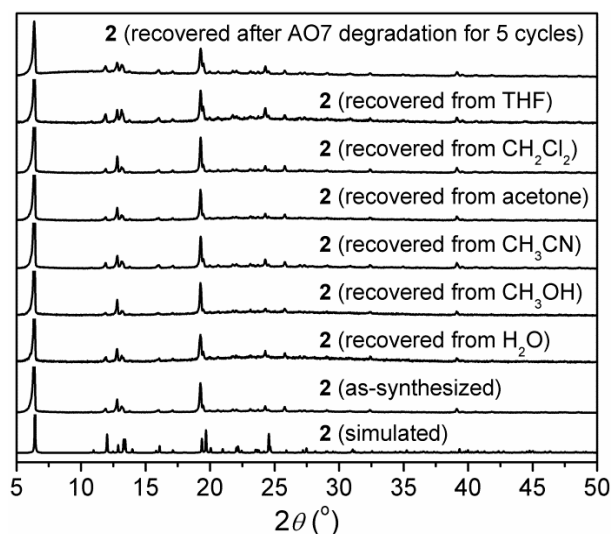


Figure 4. X-ray powder diffraction (XRPD) patterns of 2: simulated, as-synthesized, after immersing in various solvents (H<sub>2</sub>O, CH<sub>3</sub>OH, CH<sub>3</sub>CN, acetone, CH<sub>2</sub>Cl<sub>2</sub> and THF) for 1 day and after AO7 degradation experiments by H<sub>2</sub>O<sub>2</sub> for 5 cycles under daylight.

### 3.6. Photophysical Properties

In solid state, the salicyaldimine ligand, H<sub>2</sub>L<sub>salpyca</sub>, shows an unstructured fluorescence centered at 502 nm (Figure S5), upon excitation at 360 nm, which is tentatively assigned to intraligand transition [32]. Comparably, the Cu(II) complexes 1 and 2 are fluorescence silent due to the paramagnetic perturbation and/or energy/charge transfer [2,53,54].

### 3.7. Decolorization of Acid Orange 7 (AO7) Dye

Cu(II) complexes have shown the ability to various oxidation reactions including degradation of organic dyes [24,55–59]. Thus the decolorization properties of Cu(II) complexes 1 and 2 were



evaluated via photocatalytic degradation of acid orange 7 (AO7) dye, a common azo dye, under natural conditions. One milligram of Cu(II) complex (**1** or **2**) was dipped into to 3 mL of aqueous solutions of AO7 ( $20 \text{ mg L}^{-1}$ ), which was magnetically stirring in the dark for 30 min. Then, an amount of 30% hydrogen peroxide ( $\text{H}_2\text{O}_2$ , 1 mL) was added under daylight. The UV/vis spectra of the reaction solution were measured at specific intervals with a UV/vis spectrophotometer and the AO7 concentrations were determined by the maximum absorbances at 485 nm. For comparison, the same experiments were also carried out in dark conditions. In addition, several AO7 decolorization experiments examined by bare (only AO7 in  $\text{H}_2\text{O}$  without  $\text{H}_2\text{O}_2$ , **1** or **2**),  $\text{H}_2\text{O}_2$ -only, **1**-only and **2**-only were also conducted in dark conditions and under daylight. As observations, the absorbance of the major absorption band of AO7 in aqueous solutions remained almost constant in these checked decolorization experiments by bare,  $\text{H}_2\text{O}_2$ -only, **1**-only and **2**-only in dark conditions and under daylight (Figure S6a–h). The results imply that AO7 cannot be adsorbed by **1** and **2** and is very difficultly photodecomposed by daylight irradiation or oxidative/photocatalytic degradation by  $\text{H}_2\text{O}_2$  only or Cu(II) complex (**1** or **2**) only in dark conditions and even under daylight irradiation. However, the degradation of AO7 was occurred in cases of simultaneous existence of  $\text{H}_2\text{O}_2$  and Cu(II) complex (**1** or **2**) in dark conditions and under daylight, as supported by time-dependent UV/vis spectra of AO7 after degradation (Figure 5a and Figure S6i–k). In case of the simultaneous existence of **2** and  $\text{H}_2\text{O}_2$  under daylight, the aqueous solutions of AO7 showed remarkable color change from orange at initial to very light after 60-min degradation and to colorless after about 480-min degradation under daylight (Figure 5b). The findings suggest an oxidative degradation process. Of particular note, the degradation rate and the degradation performance of AO7 by **1**/ $\text{H}_2\text{O}_2$  and **2**/ $\text{H}_2\text{O}_2$  are greatly improved and enhanced under daylight in compared to that in dark conditions, implying photocatalytic degradation of AO7 by **1**/ $\text{H}_2\text{O}_2$  and **2**/ $\text{H}_2\text{O}_2$ . Moreover, the oxidative degradation ability of **2** is better than that of **1**. As a representative, the decolorization performances after 60-min degradation are about 3% and 10% for **1**/ $\text{H}_2\text{O}_2$  and **2**/ $\text{H}_2\text{O}_2$ , respectively, in dark conditions and about 10% and 85% for **1**/ $\text{H}_2\text{O}_2$  and **2**/ $\text{H}_2\text{O}_2$ , respectively, under daylight (Figure 5c). The decolorization performances would reach a maximum of approximately 15% for **1**/ $\text{H}_2\text{O}_2$  and 25% for **2**/ $\text{H}_2\text{O}_2$  in dark conditions and 25% for **1**/ $\text{H}_2\text{O}_2$  and 98% for **2**/ $\text{H}_2\text{O}_2$  under daylight. This is comparable with other cases of AO7 degradation reported in the literature [21,59–65].

To gain a better understanding of the degradation kinetics of AO7 catalyzed by **2**/ $\text{H}_2\text{O}_2$ , the experimental data were fitted by a first-order model as expressed by the following equation— $\ln(C/C_0) = kt$ —where  $C_0$  and  $C$  are the initial and apparent concentration of AO7, respectively,  $k$  is the kinetic rate constant and  $t$  is time. As a result, the  $k$  values are determined to be  $0.00291 \text{ min}^{-1}$  and  $0.0154 \text{ min}^{-1}$  for degradation of AO7 in dark conditions and under daylight (Figure 6), respectively, within 30 min. Clearly, the rate constant of AO7 degradation under daylight is about five times larger than that in dark conditions, supporting again a photocatalytic degradation of AO7. Further, there exists the first-order exponential decay relationships between the concentration of AO7 (ppm) and degradation time (min), with the formulae of  $[\text{AO7}] = 3.97 \times \exp(-t/219.85) + 15.36$  ( $R^2 = 0.93874$ ) in dark conditions and  $[\text{AO7}] = 19.52 \times \exp(-t/48.37) + 0.94$  ( $R^2 = 0.98367$ ) under daylight (Figure S7).

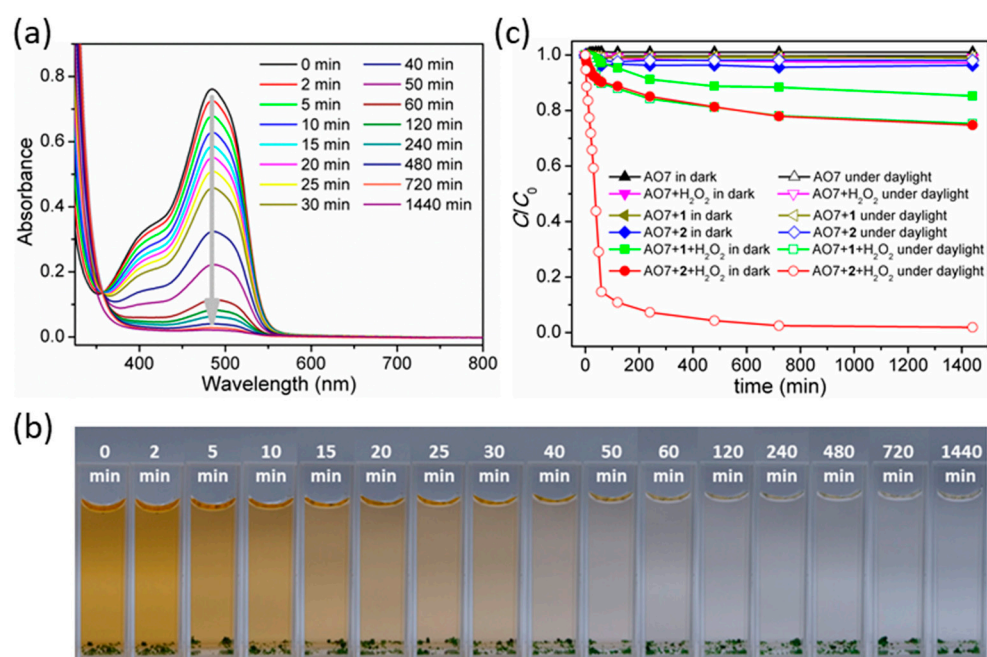


**Figure 5.** (a) Time-dependent UV/vis spectra of AO7 aqueous solution after the photocatalytic degradation by 2 and H<sub>2</sub>O<sub>2</sub> under daylight. (b) Time-dependent photographs of AO7 aqueous solutions with the simultaneous existence of 2 and H<sub>2</sub>O<sub>2</sub> under daylight. (c) Relative concentration of AO7 versus time under various degradation conditions: AO7 only in dark (▲); AO7 only under daylight (△); AO7 + H<sub>2</sub>O<sub>2</sub> in dark (▼); AO7 + H<sub>2</sub>O<sub>2</sub> under daylight (▽); AO7 + 1 in dark (◄); AO7 + 1 under daylight (◃); AO7 + 2 in dark (◆); AO7 + 2 under daylight (◇); AO7 + 1 + H<sub>2</sub>O<sub>2</sub> in dark (■); AO7 + 1 + H<sub>2</sub>O<sub>2</sub> under daylight (□); AO7 + 2 + H<sub>2</sub>O<sub>2</sub> in dark (●); AO7 + 2 + H<sub>2</sub>O<sub>2</sub> under daylight (○).

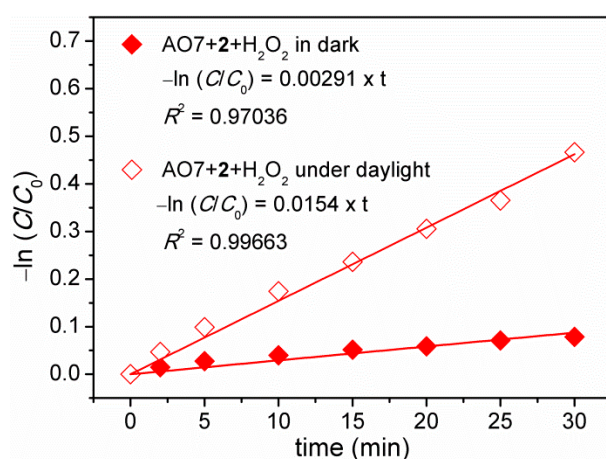


**Figure 6.** Plots of first-order kinetics model for AO7 degradation by 2/H<sub>2</sub>O<sub>2</sub> in dark conditions and under daylight.

In terms of controls, several different concentrations of 2 have been conducted to check the required concentration that shows significant photocatalytic degradation activity (Figure S8). As decreasing concentration of 2, the degradation performance decreased but still in significant extents (Figure 7). For all tested concentrations (1 mg 2 dipped into 3, 6, 15, 30 mL AO7<sub>(aq)</sub>), the photocatalytic degradation performances of AO7 are quickly increased to 33–85% within 60-min irradiation and then gradually reach to approximately 59–98% as increasing irradiation time to 1440 min. These results clearly indicated that 2 exhibits good photocatalytic activity to degrade AO7 in the presence of H<sub>2</sub>O<sub>2</sub> under daylight, even in a concentration as low as 1 mg 2/30 mL AO7<sub>(aq)</sub>.

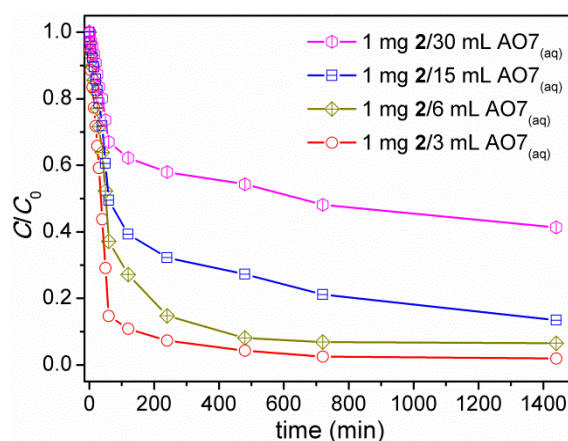


**Figure 7.** Relative concentration of AO7 versus time after the photocatalytic degradation by **2** and H<sub>2</sub>O<sub>2</sub> in different concentrations of **2** under daylight. Conditions: initial concentration of AO7 = 20 mg L<sup>-1</sup>, H<sub>2</sub>O<sub>2</sub> = 1 mL (30%).

The possible reaction mechanisms are proposed. The preliminary experiments carried out in different conditions have clearly indicated that the degradation of AO7 only taken place when Cu(II) complex (**1** or **2**) and H<sub>2</sub>O<sub>2</sub> were collaborated. In addition, the degradation performance of AO7 by **1**/H<sub>2</sub>O<sub>2</sub> and **2**/H<sub>2</sub>O<sub>2</sub> would be significantly improved (acceleration and enhancement) under daylight in compared to that in dark conditions. These observations imply that advanced oxidative processes (AOPs) [22], which is worked by the in situ generated active hydroxyl radical (<sup>•</sup>OH) as oxidizing agent to oxidatively degrade dyes, have been applied to the degradation of AO7 dye and there might be multiple pathways to dominate the AOPs. In general, the water-insoluble Cu(II) complexes can react with H<sub>2</sub>O<sub>2</sub> to produce <sup>•</sup>OH radicals via homolytic cleavage or <sup>•</sup>OH and HO<sub>2</sub><sup>•</sup> radicals via Cu redox cycles for degrading AO7 dye both in dark and under daylight [66–68]. However, daylight irradiation might result in Cu-based Fenton processes that would cause the generation of photoexcited holes (h<sup>+</sup>) and electrons (e<sup>-</sup>) [66–68]. The former might react with OH<sup>-</sup> to produce <sup>•</sup>OH whereas the latter might react with H<sub>2</sub>O<sub>2</sub> to produce <sup>•</sup>OH or O<sub>2</sub> to form O<sub>2</sub><sup>•-</sup> for oxidative degradation of AO7 dye. The formation of more active <sup>•</sup>OH, HO<sub>2</sub><sup>•</sup> and O<sub>2</sub><sup>•-</sup> radicals accelerates the whole photodegradation process and also enhances the photodegradation performances.

From the viewpoint of practices, the recycling performance and stability of photocatalysts are of particular importance during photocatalytic reactions [67]. Owing to the high decolorization performances, the recyclability and stability to leaching of **2** has been examined. Recovered powdered samples of **2** were simply washed with deionized water and MeOH several times, which were then used directly for next photocatalytic degradation experiment of AO7 (Figure S9). As observation, the photocatalytic activity of **2** toward AO7 degradation retained. The decolorization performance of **2** after 60-min degradation under daylight after five sequential experiments was slightly reduced by about 16%, giving rise to about 84% degradation efficiency of that in the first time (Figure 8, inset). However, when the irradiation time was extended over 120 min, the decolorization performances were almost unchanged (Figure 8). These results indicate that complex **2** possesses excellent long-term activity and high reusability. Noteworthy, the XRPD patterns of **2** recovered from five sequential photocatalytic degradation experiments of AO7 were in good agreement with that of as-synthesized samples (Figure 4), suggesting high stability in maintaining pristine crystalline phase. On the other hand, inductively coupled plasma optical emission spectrometry (ICP-OES) analyses indicated that there were 0.0620 ± 0.0042 mg/L of Cu(II) ions in the supernatants of AO7 aqueous solutions after 1440-min decolorization by **2** under daylight, which corresponds to 0.128 ± 0.009% Cu(II) ions leached from the solid samples of **2**. The very low ratios of Cu(II) ions in the supernatants suggests that **2** demonstrates high stability to leaching during AO7 degradation in the presence of H<sub>2</sub>O<sub>2</sub> under daylight. As a result, **2** is a good photocatalytic material toward recyclable AO7 degradation.

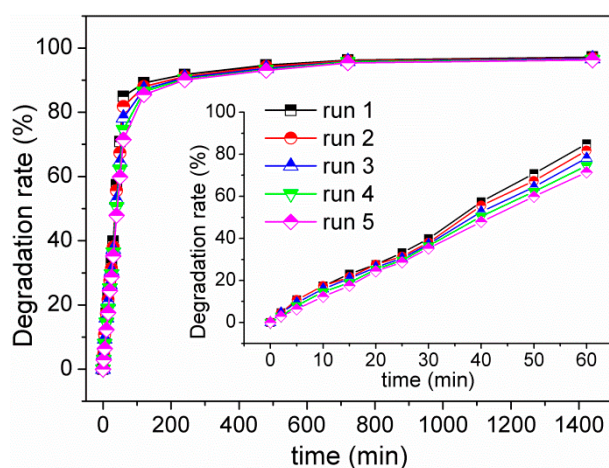


**Figure 8.** Photocatalytic degradation rates for multiple cycles for AO7 dye by 2/H<sub>2</sub>O<sub>2</sub> under daylight. Inset: Highlight the photocatalytic degradation rates within 60 min.

#### 4. Conclusions

In summary, two Cu(II)–salicyaldimine complexes have been successfully synthesized and characterized. Chloro-based complex **1** has the mononuclear structure while nitrate-containing complex **2** adopts a zigzag chain structure. The salicyaldimine ligand in the two complexes is partially deprotonated to be a mono-charged anion and acts as a NNO tris-chelator to bind a Cu(II) center through its pyridine, imino and phenolato groups and leave the neutral carboxyl group free to coordination. Noteworthy, nitrate ligand in **2** suits a bridging-tridentate with a  $\mu, \kappa^4 O, O':O'', O''$  coordination mode to bridge two Cu(II) ions, resulted in the formation of extended zigzag chain structure. The results significantly show the critical role of anions in the formation of discrete and polymeric structures of Cu(II)–salicyaldimine complexes. Moreover, **2** would be an excellent photocatalytic material to show remarkable water stability and recyclable photocatalytic degradation activity that is capable of acceleration and enhancement of AO7 decolorization by H<sub>2</sub>O<sub>2</sub> under daylight.

**Supplementary Materials:** The following are available online at <http://www.mdpi.com/2073-4360/12/9/1910/s1>, Figure S1: <sup>1</sup>H NMR spectrum of H<sub>2</sub>L<sub>salpyca</sub> in DMSO-*d*<sub>6</sub> at room temperature, Figure S2. MALDI-TOF mass spectrum of H<sub>2</sub>L<sub>salpyca</sub>, Figure S3. MALDI-TOF mass spectrum of [Cu(HL<sub>salpyca</sub>)Cl] (**1**), Figure S4. XRPD patterns of **1** and **2**, Figure S5. Solid-state excitation and emission spectra of H<sub>2</sub>L<sub>salpyca</sub> ( $\lambda_{em} = 505$  nm,  $\lambda_{ex} = 360$  nm), Figure S6. Time-dependent UV/vis spectra of AO7 aqueous solutions under various degradation conditions: (a) AO7 only in dark; (b) AO7 only under daylight, (c) AO7 + H<sub>2</sub>O<sub>2</sub> in dark; (d) AO7 + H<sub>2</sub>O<sub>2</sub> under daylight; (e) AO7 + **1** in dark; (f) AO7 + **1** under daylight; (g) AO7 + **2** in dark; (h) AO7 + **2** under daylight; (i) AO7 + **1** + H<sub>2</sub>O<sub>2</sub> in dark; (j) AO7 + **1** + H<sub>2</sub>O<sub>2</sub> under daylight; (k) AO7 + **2** + H<sub>2</sub>O<sub>2</sub> in dark, Figure S7. Concentrations of AO7 after degradation by 2/H<sub>2</sub>O<sub>2</sub> versus degradation time in dark conditions and under daylight. Solid lines show the first-order exponential decay, Figure S8. Time-dependent UV/vis spectra of AO7 aqueous solution after the photocatalytic degradation by 2/H<sub>2</sub>O<sub>2</sub> under daylight in different concentrations of **2**: (a) 1 mg **2**/6 mL AO7<sub>(aq)</sub>; (b) 1 mg **2**/15 mL AO7<sub>(aq)</sub>; (c) 1 mg **2**/30 mL AO7<sub>(aq)</sub>, Figure S9. Time-dependent UV/vis spectra of AO7 aqueous solutions for the recycling experiments with the simultaneous existence of **2** and H<sub>2</sub>O<sub>2</sub> under daylight.

**Author Contributions:** J.-Y.W. conceived and designed the experiments; M.-J.T., C.-J.T. and K.L. performed the experiments; M.-J.T. and J.-Y.W. analyzed the data; J.-Y.W. contributed reagents/materials/analysis tools; J.-Y.W. wrote the paper. All authors have read and agreed to the published version of the manuscript.

**Funding:** This research was funded by the National Chi Nan University and the Ministry of Science and Technology of Taiwan, grant number NSC 100-2113-M-260-003-MY2, NSC 102-2113-M-260-004-MY2, MOST 104-2113-M-260-005-, MOST 107-2113-M-260-001- and MOST 108-2113-M-260-002-.

**Conflicts of Interest:** The authors declare no conflict of interest.

#### References

1. Yamada, S. Advancement in stereochemical aspects of Schiff base metal complexes. *Chem. Rev.* **1999**, *190*–192, 537–555. [[CrossRef](#)]

2. Majumder, A.; Rosair, G.M.; Mallick, A.; Chattopadhyay, N.; Mitra, S. Synthesis, structures and fluorescence of nickel, zinc and cadmium complexes with the N,N,O-tridentate Schiff base N-2-pyridylmethylidene-2-hydroxy-phenylamine. *Polyhedron* **2006**, *25*, 1753–1762. [[CrossRef](#)]
3. Basak, S.; Sen, S.; Marschner, C.; Baumgartner, J.; Batten, S.R.; Turner, D.R.; Mitra, S. Synthesis, crystal structures and fluorescence properties of two new di- and polynuclear Cd(II) complexes with N<sub>2</sub>O donor set of a tridentate Schiff base ligand. *Polyhedron* **2008**, *27*, 1193–1200. [[CrossRef](#)]
4. Li, S.-N.; Zhai, Q.-G.; Hu, M.-C.; Jiang, Y.-C. Synthesis, crystal structures and characterization of three novel complexes with N-[2-(2-hydroxybenzylideneamino)ethyl]-4-methyl-benzene-sulfonamide as ligand. *Inorg. Chim. Acta* **2009**, *362*, 2217–2221. [[CrossRef](#)]
5. Gupta, K.C.; Sutar, A.K. Catalytic activities of Schiff base transition metal complexes. *Coord. Chem. Rev.* **2008**, *252*, 1420–1450. [[CrossRef](#)]
6. Zhou, X.-X.; Fang, H.-C.; Ge, Y.-Y.; Zhou, Z.-Y.; Gu, Z.-G.; Gong, X.; Zhao, G.; Zhan, Q.-G.; Zeng, R.-H.; Cai, Y.-P. Assembly of a Series of Trinuclear Zinc(II) Compounds with N<sub>2</sub>O<sub>2</sub> Donor Tetradentate Symmetrical Schiff Base Ligand. *Cryst. Growth Des.* **2010**, *10*, 4014–4022. [[CrossRef](#)]
7. Lu, Z.; Yuan, M.; Pan, F.; Gao, S.; Zhang, D.; Zhu, D. Syntheses, Crystal Structures, and Magnetic Characterization of Five New Dimeric Manganese(III) Tetradentate Schiff Base Complexes Exhibiting Single-Molecule-Magnet Behavior. *Inorg. Chem.* **2006**, *45*, 3538–3548. [[CrossRef](#)]
8. Whiteoak, C.J.; Salassa, G.; Kleij, A.W. Recent advances with  $\pi$ -conjugated salen systems. *Chem. Soc. Rev.* **2012**, *41*, 622–631. [[CrossRef](#)]
9. Escudero-Adán, E.C.; Benet-Buchholz, J.; Kleij, A.W. Expedient Method for the Transmetalation of Zn(II)-Centered Salphen Complexes. *Inorg. Chem.* **2007**, *46*, 7265–7267. [[CrossRef](#)]
10. Houjou, H.; Iwasaki, A.; Ogihara, T.; Kanetsato, M.; Akabori, S.; Hiratani, K. The architecture of dinuclear Ni and Cu complexes: Twisted and parallel forms controlled by the self-assembly of Schiff base ligands. *New J. Chem.* **2003**, *27*, 886–889. [[CrossRef](#)]
11. Yoshida, N.; Oshio, H.; Ito, T. Self-assembling tetranuclear copper(II) complex of a bis-bidentate Schiff base: Double-helical structure induced by aromatic  $\pi\cdots\pi$  and CH $\cdots\pi$  interactions. *Chem. Commun.* **1998**, 63–64. [[CrossRef](#)]
12. Kitaura, R.; Onoyama, G.; Sakamoto, H.; Matsuda, R.; Noro, S.-I.; Kitagawa, S. Immobilization of a Metallo Schiff Base into a Microporous Coordination Polymer. *Angew. Chem. Int. Ed.* **2004**, *43*, 2684–2687. [[CrossRef](#)] [[PubMed](#)]
13. Zhu, C.; Xuan, W.; Cui, Y. Luminescent microporous metal–metallo salen frameworks with the primitive cubic net. *Dalton Trans.* **2012**, *41*, 3928–3932. [[CrossRef](#)]
14. Wu, J.-Y.; Chang, C.-Y.; Tsai, C.-J.; Lee, J.-J. Reversible Single-Crystal to Single-Crystal Transformations of a Zn(II)–Salicyaldimine Coordination Polymer Accompanying Changes in Coordination Sphere and Network Dimensionality upon Dehydration and Rehydration. *Inorg. Chem.* **2015**, *54*, 10918–10924. [[CrossRef](#)] [[PubMed](#)]
15. Cho, S.-H.; Ma, B.; Nguyen, S.T.; Hupp, J.T.; Albrecht-Schmitt, T.E. A metal–organic framework material that functions as an enantioselective catalyst for olefin epoxidation. *Chem. Commun.* **2006**, 2563–2565. [[CrossRef](#)] [[PubMed](#)]
16. Jacobsen, E.N. Asymmetric Catalysis of Epoxide Ring-Opening Reactions. *Acc. Chem. Res.* **2000**, *33*, 421–431. [[CrossRef](#)]
17. Bagai, R.; Abboud, K.A.; Christou, G. Ligand-induced distortion of a tetranuclear manganese butterfly complex. *Dalton Trans.* **2006**, 3306–3312. [[CrossRef](#)]
18. Pandey, R.; Kumar, P.; Singh, A.K.; Shahid, M.; Li, P.-Z.; Singh, S.K.; Xu, Q.; Misra, A.; Pandey, D.S. Fluorescent Zinc(II) Complex Exhibiting “On-Off-On” Switching Toward Cu<sup>2+</sup> and Ag<sup>+</sup> Ions. *Inorg. Chem.* **2011**, *50*, 3189–3197. [[CrossRef](#)]
19. Anbu, S.; Ravishankaran, R.; da Silva, M.F.C.G.; Karande, A.A.; Pombeiro, A.J.L. Differentially Selective Chemosensor with Fluorescence Off–On Responses on Cu<sup>2+</sup> and Zn<sup>2+</sup> Ions in Aqueous Media and Applications in Pyrophosphate Sensing, Live Cell Imaging, and Cytotoxicity. *Inorg. Chem.* **2014**, *53*, 6655–6664. [[CrossRef](#)]
20. Iervolino, G.; Vaiano, V.; Pepe, G.; Campiglia, P.; Palma, V. Degradation of Acid Orange 7 Azo Dye in Aqueous Solution by a Catalytic-Assisted, Non-Thermal Plasma Process. *Catalysts* **2020**, *10*, 888. [[CrossRef](#)]
21. Coughlin, M.F.; Kinkle, B.K.; Bishop, P.L. Degradation of acid orange 7 in an aerobic biofilm. *Chemosphere* **2002**, *46*, 11–19. [[CrossRef](#)]

22. Zheng, J.; Gao, Z.; He, H.; Yang, S.; Sun, C. Efficient degradation of Acid Orange 7 in aqueous solution by iron ore tailing Fenton-like process. *Chemosphere* **2016**, *150*, 40–48. [[CrossRef](#)] [[PubMed](#)]
23. Guo, J.; Dong, C.; Zhang, J.; Lan, Y. Biogenic synthetic schwertmannite photocatalytic degradation of acid orange 7 (AO7) assisted by citric acid. *Sep. Purif. Technol.* **2015**, *143*, 27–31. [[CrossRef](#)]
24. Liu, C.-X.; Zhang, W.-H.; Wang, N.; Guo, P.; Muhler, M.; Wang, Y.; Lin, S.; Chen, Z.; Yang, G. Highly efficient photocatalytic degradation of dyes by a novel copper–triazolate metal–organic framework. *Chem. Eur. J.* **2018**, *24*, 16804–16813. [[CrossRef](#)]
25. Hasan, Z.; Jhung, S.H. Removal of hazardous organics from water using metal–organic frameworks (MOFs): Plausible mechanisms for selective adsorptions. *J. Hazard. Mater.* **2015**, *283*, 329–339. [[CrossRef](#)]
26. Dias, E.M.; Petit, C. Towards the use of metal–organic frameworks for water reuse: A review of the recent advances in the field of organic pollutants removal and degradation and the next steps in the field. *J. Mater. Chem. A* **2015**, *3*, 22484–22506. [[CrossRef](#)]
27. Chen, C.; Ma, W.; Zhao, J. Semiconductor-mediated photodegradation of pollutants under visible-light irradiation. *Chem. Soc. Rev.* **2010**, *39*, 4206–4219. [[CrossRef](#)]
28. Wang, C.-C.; Li, J.-R.; Lv, X.-L.; Zhang, Y.-Q.; Guo, G. Photocatalytic organic pollutants degradation in metal–organic frameworks. *Energy Environ. Sci.* **2014**, *7*, 2831–2867. [[CrossRef](#)]
29. Du, P.-Y.; Li, H.; Fu, X.; Gu, W.; Liu, X. A 1D anionic lanthanide coordination polymer as an adsorbent material for the selective uptake of cationic dyes from aqueous solutions. *Dalton Trans.* **2015**, *44*, 13752–13759. [[CrossRef](#)]
30. Yang, J.-M.; Ying, R.-J.; Han, C.-X.; Hu, Q.-T.; Xu, H.-M.; Li, J.-H.; Wang, Q.; Zhang, W. Adsorptive removal of organic dyes from aqueous solution by a Zr-based metal–organic framework: Effects of Ce(III) doping. *Dalton Trans.* **2018**, *47*, 3913–3920. [[CrossRef](#)]
31. Huang, L.; He, M.; Chen, B.; Hu, B. Magnetic Zr-MOFs nanocomposites for rapid removal of heavy metal ions and dyes from water. *Chemosphere* **2018**, *199*, 435–444. [[CrossRef](#)] [[PubMed](#)]
32. Chiang, H.-W.; Su, Y.-T.; Wu, J.-Y. Ligand dissociation/recoordination in fluorescent ionic zinc–salicylideneimine compounds: Synthesis, characterization, photophysical properties, and <sup>1</sup>H NMR studies. *Dalton Trans.* **2013**, *42*, 15169–15182. [[CrossRef](#)] [[PubMed](#)]
33. Wu, J.-Y.; Tsai, C.-J.; Chang, C.-Y.; Wu, Y.-Y. Metal-ion exchange induced structural transformation as a way of forming novel Ni(II)– and Cu(II)–salicylaldehyde structures. *J. Solid State Chem.* **2017**, *246*, 23–28. [[CrossRef](#)]
34. Tsai, M.-J.; Wu, J.-Y. Insight into the influence of framework metal ion of analogous metal–organic frameworks on the adsorptive removal performances of dyes from water. *J. Taiwan Inst. Chem. Eng.* **2019**, *102*, 73–84. [[CrossRef](#)]
35. Tsai, M.-J.; Luo, J.-H.; Wu, J.-Y. Two-fold 2D + 2D → 2D interweaved rhombus (4,4) grid: Synthesis, structure, and dye removal properties in darkness and in daylight. *Dalton Trans.* **2019**, *48*, 1095–1107. [[CrossRef](#)]
36. Tsai, M.-J.; Wu, J.-Y. Synthesis, Structure, and Dye Adsorption Properties of a Nickel(II) Coordination Layer Built from D-Camphorate and Bispyridyl Ligands. *Polymers* **2017**, *9*, 661. [[CrossRef](#)]
37. Tsai, M.-J.; Wu, J.-Y. Synthesis, characterization, and dye capture of a 3D Cd(II)–carboxylate pcu network. *Polyhedron* **2017**, *122*, 124–130. [[CrossRef](#)]
38. Williams, A.B.; Weiser, P.T.; Hanson, R.N.; Gunther, J.R.; Katzenellenbogen, J.A. Synthesis of Biphenyl Proteomimetics as Estrogen Receptor- $\alpha$  Coactivator Binding Inhibitors. *Org. Lett.* **2009**, *11*, 5370–5373. [[CrossRef](#)]
39. Song, F.; Wang, C.; Falkowski, J.M.; Ma, L.; Lin, W. Isoreticular Chiral Metal–Organic Frameworks for Asymmetric Alkene Epoxidation: Tuning Catalytic Activity by Controlling Framework Catenation and Varying Open Channel Sizes. *J. Am. Chem. Soc.* **2010**, *132*, 15390–15398. [[CrossRef](#)]
40. Sheldrick, G.M. A short history of SHELX. *Acta Crystallogr. Sect. A* **2008**, *64*, 112–122. [[CrossRef](#)]
41. Sheldrick, G.M. Crystal structure refinement with SHELXL. *Acta Crystallogr. Sect. C* **2015**, *71*, 3–8. [[CrossRef](#)] [[PubMed](#)]
42. Farrugia, L.J. WinGX and ORTEP for Windows: An update. *J. Appl. Crystallogr.* **2012**, *45*, 849–854. [[CrossRef](#)]
43. Brandenburg, K.; Putz, H. *Diamond; Crystal Impact GbR*: Bonn, Germany, 1999.
44. Etter, M.C. Encoding and decoding hydrogen-bond patterns of organic compounds. *Acc. Chem. Res.* **1990**, *23*, 120–126. [[CrossRef](#)]
45. Addison, A.W.; Rao, T.N.; Reedijk, J.; van Rijn, J.; Verschoor, G.C. Synthesis, structure, and spectroscopic properties of copper(II) compounds containing nitrogen–sulphur donor ligands; the crystal and molecular

- structure of aqua[1,7-bis(*N*-methylbenzimidazol-2'-yl)-2,6-dithiaheptane]copper(II) perchlorate. *J. Chem. Soc. Dalton Trans.* **1984**, 1349–1356. [[CrossRef](#)]
46. Addison, C.C.; Logan, N.; Wallwork, S.C.; Garner, C.D. Structural Aspects of Co-ordinated Nitrate Groups. *Q. Rev. Chem. Soc.* **1971**, *25*, 289–322. [[CrossRef](#)]
  47. Jianmin, L.; Huaqianga, Z.; Yugenb, Z.; Jinhua, C.; Yanxiong, K.; Quanming, W.; Xintao, W. The Crystal Structure of [La(NO<sub>3</sub>)<sub>6</sub>{Cu(2,2'-bipy)<sub>2</sub>}<sub>2</sub>][La(NO<sub>3</sub>)<sub>6</sub>Cu(2,2'-bipy)<sub>2</sub>]-CH<sub>3</sub>CN with the Most Profuse Modes of Nitrate Coordination. *Cryst. Res. Technol.* **1999**, *34*, 925–928. [[CrossRef](#)]
  48. Banu, K.S.; Ghosh, T.; Guha, A.; Chattopadhyay, T.; Das, D.; Zangrando, E. Structure and luminescence of a nitrate-bridged heterotrimeric Cu<sub>2</sub>-Pr complex with compartmental Schiff base ligand. *J. Coord. Chem.* **2010**, *63*, 3714–3723. [[CrossRef](#)]
  49. Ling, J.; Ozga, M.; Stoffer, M.; Burns, P.C. Uranyl peroxide pyrophosphate cage clusters with oxalate and nitrate bridges. *Dalton Trans.* **2012**, *41*, 7278–7284. [[CrossRef](#)]
  50. Chaudhari, A.K.; Joarder, B.; Rivière, E.; Rogez, G.; Ghosh, S.K. Nitrate-Bridged “Pseudo-Double-Propeller”-Type Lanthanide(III)–Copper(II) Heterometallic Clusters: Syntheses, Structures, and Magnetic Properties. *Inorg. Chem.* **2012**, *51*, 9159–9161. [[CrossRef](#)]
  51. She, S.; Chen, Y.; Zaworotko, M.J.; Liu, W.; Cao, Y.; Wu, J.; Li, Y. Synthesis, structures and magnetic properties of a family of nitrate-bridged octanuclear [Na<sub>2</sub>Ln<sub>6</sub>] (Ln = Dy, Tb, Gd, Sm) complexes. *Dalton Trans.* **2013**, *42*, 10433–10438. [[CrossRef](#)]
  52. Morozov, I.V.; Serezhkin, V.N.; Troyanov, S.I. Modes of coordination and stereochemistry of the NO<sub>3</sub><sup>−</sup> anions in inorganic nitrates. *Russ. Chem. Bull. Int. Ed.* **2008**, *57*, 439–450. [[CrossRef](#)]
  53. Senthilkumar, S.; Goswami, R.; Smith, V.J.; Bajaj, H.C.; Neogi, S. Pore Wall-Functionalized Luminescent Cd(II) Framework for Selective CO<sub>2</sub> Adsorption, Highly Specific 2,4,6-Trinitrophenol Detection, and Colorimetric Sensing of Cu<sup>2+</sup> Ions. *ACS Sustain. Chem. Eng.* **2018**, *6*, 10295–10306. [[CrossRef](#)]
  54. Udhayakumari, D.; Velmathi, S.; Sung, Y.-M.; Wu, S.-P. Highly fluorescent probe for copper (II) ion based on commercially available compounds and live cell imaging. *Sens. Actuators B Chem.* **2014**, *198*, 285–293. [[CrossRef](#)]
  55. Yang, H.; He, X.-W.; Wang, F.; Kang, Y.; Zhang, J. Doping copper into ZIF-67 for enhancing gas uptake capacity and visible-light-driven photocatalytic degradation of organic dye. *J. Mater. Chem.* **2012**, *22*, 21849–21851. [[CrossRef](#)]
  56. Wen, T.; Zhang, D.-X.; Zhang, J. Two-Dimensional Copper(I) Coordination Polymer Materials as Photocatalysts for the Degradation of Organic Dyes. *Inorg. Chem.* **2013**, *52*, 12–14. [[CrossRef](#)]
  57. Sun, X.; Zhang, J.; Fu, Z. Polyoxometalate Cluster Sensitized with Copper-Viologen Framework for Efficient Degradation of Organic Dye in Ultraviolet, Visible, and Near-Infrared Light. *ACS Appl. Mater. Interfaces* **2018**, *10*, 35671–35675. [[CrossRef](#)]
  58. Peng, Y.-F.; Qian, L.-L.; Ding, J.-G.; Zheng, T.-R.; Zhang, Y.-Q.; Li, B.-L. Syntheses, structures and photocatalytic degradation of organic dyes for two isostructural copper coordination polymers involving in situ hydroxylation reaction. *J. Coord. Chem.* **2018**, *71*, 1392–1402. [[CrossRef](#)]
  59. Hou, Y.-L.; Sun, R.W.-Y.; Zhou, X.-P.; Wang, J.-H.; Li, D. A copper(I)/copper(II)–salen coordination polymer as a bimetallic catalyst for three-component Strecker reactions and degradation of organic dyes. *Chem. Commun.* **2014**, *50*, 2295–2297. [[CrossRef](#)]
  60. Wu, J.; Zhang, H.; Qiu, J. Degradation of Acid Orange 7 in aqueous solution by a novel electro/Fe<sup>2+</sup>/peroxydisulfate process. *J. Hazard. Mater.* **2012**, *215–216*, 138–145. [[CrossRef](#)]
  61. Piumetti, M.; Freyria, F.S.; Armandi, M.; Saracco, G.; Garrone, E.; Gonzalez, G.E.; Bonelli, B. Catalytic degradation of Acid Orange 7 by H<sub>2</sub>O<sub>2</sub> as promoted by either bare or V-loaded titania under UV light, in dark conditions, and after incubating the catalysts in ascorbic acid. *Catal. Struct. React.* **2015**, *1*, 183–191. [[CrossRef](#)]
  62. Ji, P.; Zhang, J.; Chen, F.; Anpo, M. Study of adsorption and degradation of Acid Orange 7 on the surface of CeO<sub>2</sub> under visible light irradiation. *Appl. Catal. B* **2009**, *85*, 148–154. [[CrossRef](#)]
  63. Elías, V.; Vaschetto, E.; Sapag, K.; Oliva, M.; Casuscelli, S.; Eimer, G. MCM-41-based materials for the photo-catalytic degradation of Acid Orange 7. *Catal. Today* **2011**, *172*, 58–65. [[CrossRef](#)]
  64. Yin, C.; Zhao, C.; Xu, X.-J. Crystal structure and photocatalytic degradation properties of a new two-dimensional zinc coordination polymer based on 4,4'-oxy-bis(benzoic acid). *Z. Naturforsch.* **2019**, *74*, 861–864. [[CrossRef](#)]

65. Wang, F.; Li, F.-L.; Xu, M.-M.; Yu, H.; Zhang, J.-G.; Xia, H.-T.; Lang, J.-P. Facile synthesis of a Ag(I)-doped coordination polymer with enhanced catalytic performance in the photodegradation of azo dyes in water. *J. Mater. Chem. A* **2015**, *3*, 5908–5916. [[CrossRef](#)]
66. Li, J.; Pham, A.N.; Dai, R.; Wang, Z.; Waite, T.D. Recent advances in Cu-Fenton systems for the treatment of industrial wastewaters: Role of Cu complexes and Cu composites. *J. Hazard. Mater.* **2020**, *392*, 122261. [[CrossRef](#)]
67. Wang, D.; Zhao, P.; Yang, J.; Xu, G.; Yang, H.; Shi, Z.; Hu, Q.; Dong, B.; Guo, Z. Photocatalytic degradation of organic dye and phytohormone by a Cu(II) complex powder catalyst with added H<sub>2</sub>O<sub>2</sub>. *Colloids Surf. A* **2020**, *603*, 125147. [[CrossRef](#)]
68. Carvalho, S.S.F.; Rodrigues, A.C.C.; Lima, J.F.; Carvalho, N.M.F. Photocatalytic degradation of dyes by mononuclear copper(II) complexes from bis-(2-pyridylmethyl)amine NNN-derivative ligands. *Inorg. Chim. Acta* **2020**, *512*, 119924. [[CrossRef](#)]



© 2020 by the authors. Licensee MDPI, Basel, Switzerland. This article is an open access article distributed under the terms and conditions of the Creative Commons Attribution (CC BY) license (<http://creativecommons.org/licenses/by/4.0/>).